Characterization of semiconductor-laser phase noise and estimation of bit-error rate performance with low-speed offline digital coherent receivers

Kazuro Kikuchi*

Department of Electrical Engineering and Information Systems, The University of Tokyo
7-3-1 Hongo, Bunkyo-Ku, Tokyo 113-8656, Japan

**kikuchi@ginjo.t.u-tokyo.ac.jp*

Abstract: We develop a systematic method for characterizing semiconductor-laser phase noise, using a low-speed offline digital coherent receiver. The field spectrum, the FM-noise spectrum, and the phase-error variance measured with such a receiver can completely describe phase-noise characteristics of lasers under test. The sampling rate of the digital coherent receiver should be much higher than the phase-fluctuation speed. However, 1 GS/s is large enough for most of the single-mode semiconductor lasers. In addition to such phase-noise characterization, interpolating the taken data at 1.25 GS/s to form a data stream at 10 GS/s, we can predict the bit-error rate (BER) performance of multi-level modulated optical signals at 10 Gsymbol/s. The BER degradation due to the phase noise is well explained by the result of the phase-noise measurements.

OCIS codes: (060.2330) Fiber optics communications; (060.1660) Coherent communications; (060.2920) Homodyning.

References and links

1. M. G. Taylor, "Coherent detection method using DSP for demodulation of signal and subsequent equalization of propagation impairments," IEEE Photon. Technol. Lett. **16**, 674–676 (2004).
2. K. Kikuchi, "Phase-diversity homodyne detection of multi-level optical modulation with digital carrier phase estimation," IEEE J. Sel. Top. Quantum Electron. **12**, 563–570 (2006).
3. K. Kikuchi, "Digital coherent optical communication systems: Fundamentals and future prospects," IEICE Electron. Express **8**, 1642–1662 (2011).
4. A.H. Gnauck, P. J. Winzer, S. Chandrasekhar, X. Liu, B. Zhu, and D. W. Peckham, "10×224-Gb/s WDM transmission of 28-Gbaud PDM 16-QAM on a 50-GHz grid transmission over 1,200 km of fiber," in 2010 OSA Technical Digest of *Optical Fiber Communication Conference* (Optical Society of America, 2010), PDPB8.
5. A. Sano, T. Kobayashi, K. Ishihara, H. Masuda, S. Yamamoto, K. Mori, E. Yamazaki, E. Yoshida, Y. Miyamoto, T. Yamada, and H. Yamazaki, "240-Gb/s polarization-multiplexed 64-QAM modulation and blind detection using PLC-LN hybrid integrated modulator and digital coherent receiver," European Conference on Optical Communication, Sept. 2009, Vienna, Austria, PD2.2.
6. K. Kikuchi, "Analyses of wavelength- and polarization-division multiplexed transmission characteristics of optical quadrature-amplitude-modulation signals," Opt. Express **19**, 17985–17995 (2011).
7. R. Nagarajan, D. Lambert, M. Kato, V. Lal, G. Goldfarb, J. Rahn, M. Kuntz, J. Pleumeekers, A. Dentai, H.-S. Tsai, R. Malendevich, M. Missey, K.-T. Wu, H. Sun, J. McNicol, J. Tang, J. Zhang, T. Butrie, A. Nilsson, M. Reffle, F. Kish, and D. Welch, "10 channel, 100Gbit/s per channel, dual polarization, coherent QPSK, monolithic InP receiver photonic integrated circuit," in 2011 OSA Technical Digest of *Optical Fiber Communication Conference* (Optical Society of America, 2011), OML7.
8. T. Okoshi and K. Kikuchi, *Coherent Optical Communication Systems* (KTK/Kluwer, 1988), Chap.3.

#160727 - $15.00 USD Received 3 Jan 2012; revised 2 Feb 2012; accepted 13 Feb 2012; published 17 Feb 2012

9. K. Kikuchi, T. Okoshi, M. Nagamatsu, and N. Henmi, "Degradation of bit-error rate in coherent optical communications due to spectral spread of the transmitter and the local oscillator," J. Lightwave Technol. **2**, 1024–1033 (1984).
10. K. Kikuchi, "Impact of 1/f-type FM noise on coherent optical communications," Electron. Lett. **23**, 885–887 (1987).
11. K. Kikuchi and T. Okoshi, "Measurement of FM noise, AM noise, and field spectra of 1.3μm InGaAsP DFB lasers and determination of the linewidth enhancement factor," IEEE J. Quantum Electron. **21**, 1814–1818 (1985).
12. K. Kikuchi and K. Igarashi, "Characterization of semiconductor-laser phase noise with digital coherent receivers," in 2011 OSA Technical Digest of *Optical Fiber Communication Conference* (Optical Society of America, 2011), OML3.
13. R. Maher and B. Thomsen, "Dynamic linewidth measurement technique using digital intradyne coherent receivers," Opt. Express **19**, B313–B322 (2011).
14. A. J. Viterbi and A. N. Viterbi, "Nonlinear estimation of PSK-modulated carrier phase with application to burst digital transmission," IEEE Trans. Inf. Theory **29**, 543–551 (1983).
15. M. Seimetz, "Laser linewidth limitations for optical systems with high-order modulation employing feed forward digital carrier phase estimation," in 2008 OSA Technical Digest of *Optical Fiber Communication Conference* (Optical Society of America, 2008), NWA4.

1. Introduction

With the recent development of digital coherent receivers [1–3], multi-level modulation formats have attracted large attention because of their spectrally-efficient transmission characteristics in polarization- and wavelength-division multiplexed (WDM) systems [4–6]. In such systems, phase-noise characteristics of lasers for the transmitter and the local oscillator (LO) strongly affect the bit-error rate (BER) performance. We are usually concerned about the 3-dB spectral width of lasers for the transmission system design. However, the 3-dB spectral width is dependent on the measurement method and is not necessarily a good measure of the phase noise of lasers. In order to characterize the coherent transmitter and receiver [7], it is a crucial consideration to establish a standard method of phase-noise measurements.

In this paper, we present a systematic method for fully characterizing the laser phase noise, using a low-speed offline digital coherent receiver. The digital coherent receiver acquires the complex amplitude of a beat between two lasers, from which we can evaluate the field spectrum, the FM-noise spectrum, and the phase-error variance though offline digital signal processing. The sampling rate of the digital coherent receiver should be much higher than the phase-fluctuation speed. However, 1 GS/s is large enough for characterizing the phase noise of most of the single-mode semiconductor lasers such as distributed-feedback (DFB) laser, distributed Bragg-reflector (DBR) lasers, and external-cavity lasers. The offline signal processing and the relatively low sampling rate of the digital coherent receiver make it easier to construct the experimental setup.

Using the proposed method, we measure the phase-noise characteristics of DFB and DBR semiconductor lasers. The 3-dB spectral width of the lasers has a dependence on the measurement time, whose origin can be analyzed using the FM-noise spectrum, the phase-noise variance, and the time-resolved field spectrum. Interpolating the data of the complex amplitude taken at 1.25 GS/s to form a 10-GS/s data stream, we can also calculate the BER performance of the 10-Gsymbol/s quadrature phase-shift keying (QPSK) system and the 16 quadrature-amplitude-modulation (QAM) system, where these lasers are used as the transmitter and LO. The BER degradation due to the phase noise is well explained by the measured FM-noise spectrum.

The organization of this paper is as follows: Section 2 describes the method of phase-noise evaluation, which includes the theoretical basis of characterization of the laser phase noise and the proposed experimental setup. In Sec.3, we present experimental results on the phase-noise measurements of DFB and DBR semiconductor lasers. Section 4 deals with the BER performance of 10-Gsymbol/s QPSK and 16-QAM signals calculated from the 1.25-GS/s data.

#160727 - $15.00 USD Received 3 Jan 2012; revised 2 Feb 2012; accepted 13 Feb 2012; published 17 Feb 2012

Section 5 concludes the paper.

2. Evaluation method of phase-noise characteristics

2.1. Functions characterizing the phase noise

Figure 1 shows relations among the complex amplitude $E(t)$ of the laser under test, the phase difference $\Delta\phi_\tau(t)$, the field spectrum $S(f)$, the FM-noise spectrum $S_F(t)$, and the phase-error variance $\sigma_\phi(\tau)^2$. Equations (1)-(6) in Fig. 1, which relate those to each other, are listed in Table 1 [8]. As shown in Fig. 1, we measure $E(t)$ by a digital coherent receiver and calculate the three functions, the field spectrum $S(f)$, the FM-noise spectrum $S_F(f)$, and the phase-error variance $\sigma(\tau)^2$, using Eqs.(1)-(6) in Table 1. These functions are applied to characterizing the phase noise.

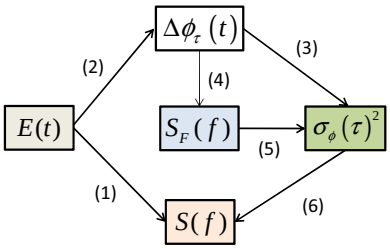

Fig. 1. Relations among the complex amplitude $E(t)$, the phase difference $\Delta\phi_\tau(t)$, the field spectrum $S(f)$, the FM-noise spectrum $S_F(t)$, and the phase-error variance $\sigma_\phi(\tau)^2$. Equations (1)-(6) relating those to each other are listed in Table 1.

Table 1. Equations relating the complex amplitude $E(t)$, the phase difference $\Delta\phi_\tau(t)$, the field spectrum $S(f)$, the FM-noise spectrum $S_F(t)$, and the phase-error variance $\sigma_\phi(\tau)^2$ to each other. $\mathscr{F}[*]$ represents the Fourier transform, and $\langle * \rangle$ the ensemble average.

Equation	Eq. Number
$S(f) = \langle \lvert \mathscr{F}[E(t)] \rvert^2 \rangle$	(1)
$\Delta\phi_\tau(t) = \phi_n(t) - \phi_n(t-\tau)$	(2)
$\sigma_\phi(\tau)^2 = \langle \Delta\phi_\tau(t)^2 \rangle$	(3)
$S_{\Delta\phi_\tau}(f) = 4\left(\frac{\sin(\pi f\tau)}{f}\right)^2 S_F(f)$	(4)
$\sigma_\phi(\tau)^2 = 4\int_0^\infty \left(\frac{\sin(\pi f\tau)}{f}\right)^2 S_F(f)\,df$	(5)
$S(f) = \mathscr{F}\left[\exp\left(-\frac{\sigma_\phi(\tau)^2}{2}\right)\right]$	(6)

#160727 - $15.00 USD Received 3 Jan 2012; revised 2 Feb 2012; accepted 13 Feb 2012; published 17 Feb 2012

Let the complex amplitude of the optical signal be $E(t)$. The field spectrum $S(f)$ is defined as the power-spectral-density function of $E(t)$ as shown by Eq. (1) in Table 1. Since the AM noise of semiconductor lasers operating well above threshold is negligibly small, the spectral width of $S(f)$ mainly stems from the phase noise and is the most common measure of the phase noise.

When the AM noise is neglected, the phase noise is approximately given as the argument of $E(t)$:

$$\phi_n(t) = \arg\left(E(t)\right). \tag{7}$$

The phase difference $\Delta\phi_\tau(t)$ generated in a time interval τ is given as Eq. (2). Then, the phase-error variance $\sigma_\phi(\tau)^2$, which is the mean-square value of such phase difference, is obtained from Eq. (3). The slope of the τ-versus-$\sigma_\phi(\tau)^2$ characteristics is another measure of the phase noise. Especially in differentially coherent detection schemes such as differential phase-shift keying (DPSK) and differential quadrature PSK (DQPSK) schemes, $\sigma_\phi(T)^2$ can directly determine the BER performance where T denotes the symbol duration [9].

On the other hand, the instantaneous-frequency fluctuation can be approximated as

$$f_i(t) = \frac{\Delta\phi_\tau(t)}{2\pi\tau}, \tag{8}$$

when τ is small enough. The FM-noise spectrum $S_F(t)$ means the power-spectral-density function of $f_i(t)$. It is calculated from $S_{\Delta\phi_\tau}(f)$, which is the the power-spectral-density function of $\Delta\phi_\tau(t)$, as seen from Eq. (4). These functions, $S(f)$, $\sigma_\phi(\tau)^2$, and $S_F(f)$, are related to each other through Eqs. (5) and (6). We find that the FM-noise spectrum is the most fundamental function for evaluating the phase noise, because both of $S(f)$ and $\sigma_\phi(\tau)^2$ are derived from $S_F(f)$.

2.2. Typical examples of the relation among the field spectrum, the FM-noise spectrum, and the phase-error variance

It is worthy of mentioning the ideal case where the FM noise is white and its single-sided spectral density is expressed as

$$S_F(f) = \frac{\delta f}{\pi}. \tag{9}$$

In such a case, the phase-error variance $\sigma_\phi(\tau)^2$ is given from Eq. (5) as

$$\sigma_\phi(\tau)^2 = 2\pi\delta f\tau. \tag{10}$$

Note that the phase-error variance is linearly proportional to τ. Then, Eq. (6) leads to the double-sided field spectrum having the Lorentzian shape as

$$S(f) = \frac{\delta f}{2\pi\left[f^2 + \left(\frac{\delta f}{2}\right)^2\right]}. \tag{11}$$

Thus, we find that δf in Eq. (9) represents the 3-dB linewidth of the field spectrum $S(f)$. Figure 2 illustrates (a) $S_F(f)$, (b) $\sigma_\phi(\tau)^2$, and (c) $S(f)$ in the ideal case. Using only one parameter of δf, we can fully describe the phase-noise characteristics. Such ideal case is usually assumed in the coherent system design.

However, in actual cases the FM-noise spectrum is not necessarily flat, but its spectral density is often enhanced in the low-frequency region as shown by the red arrow in Fig. 3 (a) [10]. The phase-error variance in such cases deviates from the linear relation with respect to τ (Fig. 3(b)). Then, the field spectrum is dependent on the measurement time as discussed in what

#160727 - $15.00 USD Received 3 Jan 2012; revised 2 Feb 2012; accepted 13 Feb 2012; published 17 Feb 2012

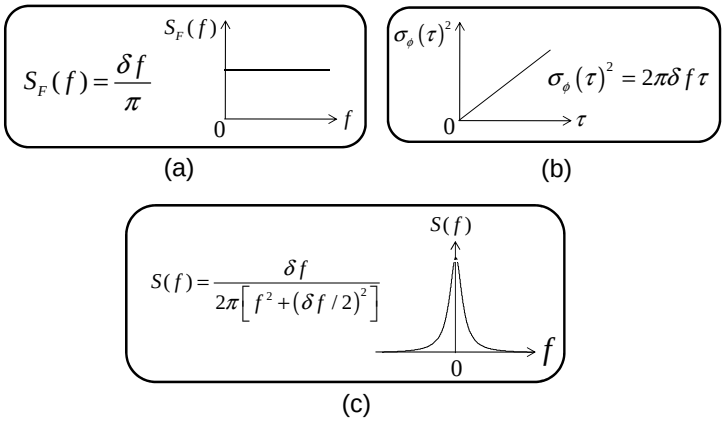

Fig. 2. (a) FM noise spectrum $S_F(f)$, (b) phase-error variance $\sigma_\phi(\tau)^2$, and (c) $S(f)$ in the ideal case where the FM noise is white.

follows: The Lorentzian lineshape determined from the white FM noise is measured only when the measurement time interval is short enough; however, the center frequency of the Lorentzian spectrum drifts because of instantaneous-frequency fluctuations in the low frequency side, as the measurement time becomes longer. Such frequency drift results in a broadened field spectrum as shown in Fig. 3(c). This fact means that the 3-dB linewidth of $S(f)$ is no more a good measure of the phase noise since it is dependent on the measurement time. Therefore, for the coherent system design, we need the information on $S_F(f)$.

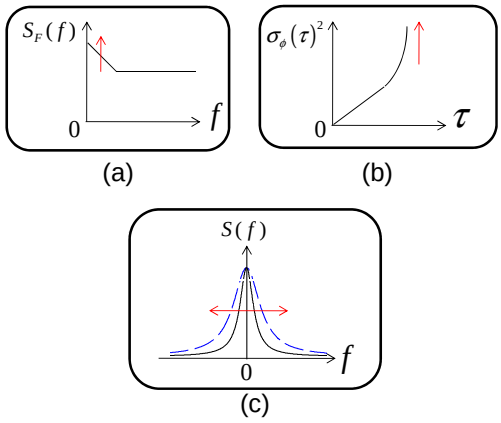

Fig. 3. (a) FM noise spectrum $S_F(f)$, (b) phase-error variance $\sigma_\phi(\tau)^2$, and (c) $S(f)$ in the case where the low-frequency FM noise is enhanced.

2.3. Experimental setup for phase-noise characterization

Figure 4 shows the experimental setup for phase-noise characterization. Instead of phase-noise measurements in the optical domain [11], we use a digital coherent receiver [12], [13], which down-converts the optical signal to the electrical signal, and analyze the phase-noise characteristics in the electrical domain.

The digital coherent receiver consists of the phase-diversity optical circuit, the LO laser for homodyne detection, the analog-to-digital converter (ADC), and the digital signal processor

#160727 - $15.00 USD Received 3 Jan 2012; revised 2 Feb 2012; accepted 13 Feb 2012; published 17 Feb 2012

(DSP). The state of polarization of the signal is aligned to that of the LO. The receiver detects a beat between the signal laser under test and the LO.

The in-phase (I) and quadrature (Q) components of the complex amplitude of the received beat signal are sent to the two-channel ADC and processed offline on the personal computer (PC). We can thus obtain the phase-noise characteristics of the beat signal, namely, $S(f)$, $\sigma_\phi(\tau)^2$, and $S_F(f)$, all at once. In contrast to the receiver for optical communications, our receiver can operate offline for phase-noise analyses.

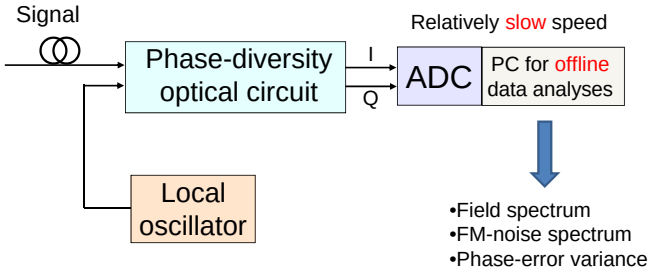

Fig. 4. Experimental setup of a digital coherent receiver, which consists of a phase-diversity optical circuit, an LO, and a digital signal processor. The complex amplitude of the beat signal is sampled by a two-channel analog-to-digital converter (ADC) and processed by an offline personal computer (PC).

3. Experimental Results

First, we measured the phase-noise characteristics of narrow-linewidth DFB semiconductor lasers (NEL, DFB NLK1564STB), which were used for the signal and the LO. These lasers had similar characteristics and their center wavelengths were around 1550 nm.

Black curves in Figs. 5(a), 5(b), and 5(c) show the field spectrum $S(f)$, the FM-noise spectrum $S_F(f)$, and the phase-error variance $\sigma_\phi(\tau)^2$ of the beat between the two DFB lasers, respectively. The sampling rate was $1/\tau_s = 1.25$ GS/s and the number of samples $n = 1.25 \times 10^5$. Then, the measurement time in this case was $\tau_s n = 10^{-4}$ s. The offset frequency of the beat was maintained less than 10 MHz. From Fig. 5(c), we find that the phase-error variance is proportional to the delay time τ, as shown by the red broken line fitted to the experimental result. Noting that the slope of the red broken line is $2\pi\delta f$ in the ideal case (Eq. (10)), we can estimate that $\delta f = 170$ kHz, which means that the linewidth of each laser is 85 kHz if linewidths of the two lasers are equal. Then, we can draw a Lorentzian shape with $\delta f = 170$ kHz shown by the red curve in Fig. 5(a) (Eq. (11)), which is in perfect agreement with the experimental result over a range of 40 dB. On the other hand, Fig. 5(b) shows that the FM-noise spectrum is approximately white, and the red line represents its spectral density obtained from the linewidth as $\delta f/\pi$ (Eq. (9)), which is also in good agreement with the experimental result.

On the other hand, black curves in Fig. 6 show the phase-noise characteristics measured when the IQ data were directly sampled at $1/\tau_s = 12.5$ MS/s and the number of the samples was $n = 1.25 \times 10^5$. The measurement time $\tau_s n$ was extended to 10^{-2} s. The offset frequency of the beat was kept below 1 MHz. Since the spectral width in Fig. 6(a) is still much smaller than the sampling rate, the spectrum folding due to the aliasing effect is not significant. In this case, we clearly find that the phase-noise characteristics deviate from the ideal ones shown in Fig. 2 due to low-frequency FM noise [10]. The red broken line in Fig. 6(c) represents the linear fit to the experimental phase-error variance in the small delay-time region. The red line in Fig. 6(b) is the spectral density of the FM noise obtained from the slope of the fitted line in Fig. 6(c). It is seen that the FM-noise spectral density increases in the lower frequency side, whereas it is flat

#160727 - $15.00 USD Received 3 Jan 2012; revised 2 Feb 2012; accepted 13 Feb 2012; published 17 Feb 2012

in the high-frequency side. The flat spectral density is in good agreement with the red line. The Lorentzian spectrum calculated from the flat FM-noise component in Fig. 6(b) is shown by the red curve in Fig. 6(a), which differs from the measured one significantly.

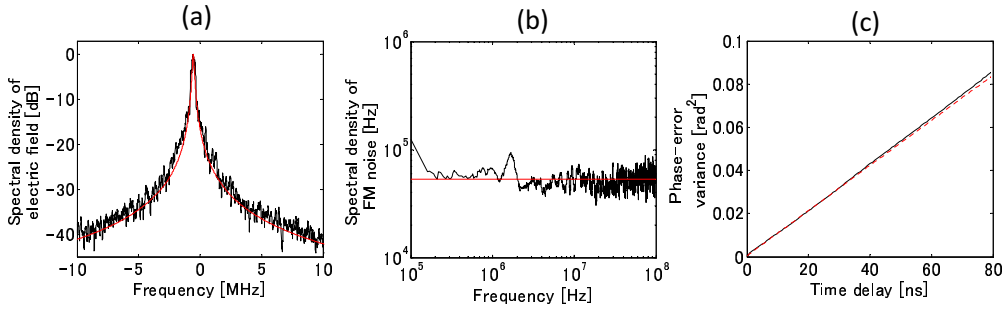

Fig. 5. (a) Field spectrum $S(f)$, (b) FM-noise spectrum $S_F(f)$, and (c) phase-error variance $\sigma_\phi(\tau)^2$ of the beat between the signal and LO, when $1/\tau_s = 1.25$ GS/s and $n = 1.25\times10^5$. Red curves are theoretical fits using Eqs. (9), (10), and (11).

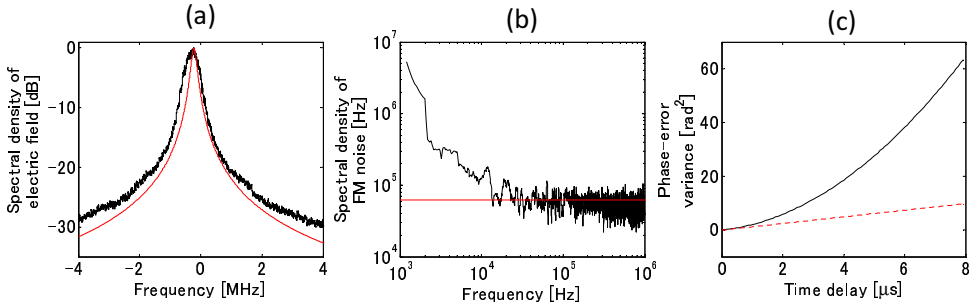

Fig. 6. (a) Field spectrum $S(f)$, (b) FM-noise spectrum $S_F(f)$, and (c) phase-error variance $\sigma_\phi(\tau)^2$ of the beat between the signal and LO, when $1/\tau_s = 12.5$ MS/s and $n = 1.25\times10^5$. The measurement time is 100 times longer than that in Fig. 5. Red curves are theoretical fits using Eqs. (9), (10), and (11).

In order to examine the effect of the low-frequency FM noise more clearly, we calculate time-resolved field spectra as follows: The total measurement time of 10^{-2} is divided into ten sections having 10^{-3}-s time intervals, and the field spectrum in each section is calculated in time order from 1×10^{-3} s to 10×10^{-3} s. Figure 7 shows such time-resolved field spectra. The range of the vertical axis is limited to 15 dB in order to show only the center-frequency fluctuation. We find that the center frequency of the spectrum measured in the shorter time interval of 10^{-3} s fluctuates significantly, resulting in a broadened spectrum measured in the longer time interval of 10^{-2} s.

In high bit-rate systems, the white FM-noise component mainly determines the BER performance; however, the 3-dB spectral width does not necessarily correspond to it. For complete characterization of phase noise, it is important to evaluate the field spectrum, FM-noise spectrum, and phase-error variance simultaneously, changing the measurement time.

Next, we measured the phase-noise characteristics of a DBR semiconductor laser. The LO laser was one of the DFB lasers which were used in the previous experiment. Since the phase noise of the DBR laser is much larger than that of the DFB laser, we can consider that the phase noise of the beat is almost identical with that of the DBR laser.

#160727 - $15.00 USD Received 3 Jan 2012; revised 2 Feb 2012; accepted 13 Feb 2012; published 17 Feb 2012

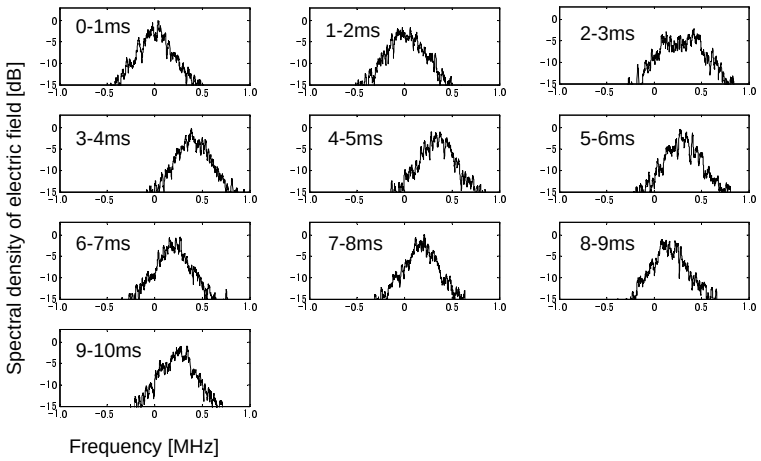

Fig. 7. Time-resolved field spectra. The total measurement time of 10^{-2} s is divided into ten sections having 10^{-3}-s time intervals, and the field spectrum in each section is calculated in time order from 1×10^{-3} s to 10×10^{-3} s.

Black curves in Figs. 8(a), 8(b), and 8(c) show the field spectrum $S(f)$, the FM-noise spectrum $S_F(f)$, and the phase-error variance $\sigma_\phi(\tau)^2$ of the DBR laser, respectively. The sampling rate was $1/\tau_s = 1.25$ GS/s and the number of samples was $n = 1.25\times10^5$. As seen from Figs. 5(b) and 8(b), the low-frequency FM noise of the DBR laser is much larger than that of the DFB laser. The passive phase-control region in the DBR laser most likely generates such low-frequency FM noise, which may be reduced by a current source with lower electrical noise [13]. The red broken line in Fig. 8(c) represents the linear fit to the experimental phase-error variance in the small delay-time region. The red line in Fig. 8(b) is the spectral density of the FM noise obtained from the slope of the fitted line in Fig. 8(c). The FM-noise spectrum is flat in the high-frequency side, and the flat spectral density is in good agreement with the red line. The Lorentzian spectrum calculated from the flat FM-noise component in Fig. 8(b) is shown by the red curve in Fig. 8(a). The 3-dB width of the measured spectrum is much larger than that of the calculated Lorentzian spectrum, which is about 600 kHz. We find that the low-frequency FM noise broadens the field spectrum significantly. Such excess spectral broadening of the DBR laser is much larger than that of the DFB laser.

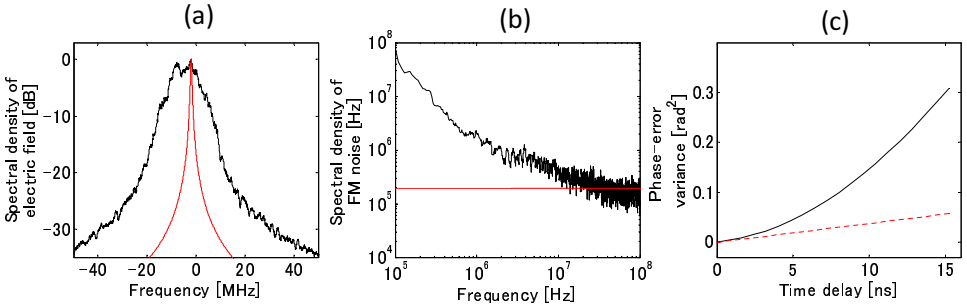

Fig. 8. (a) Field spectrum $S(f)$, (b) FM-noise spectrum $S_F(f)$, and (c) phase-error variance $\sigma_\phi(\tau)^2$ of the DBR laser, when $1/\tau_s = 1.25$ GS/s and $n = 1.25\times10^5$. Red curves are theoretical fits using Eqs. (9), (10), and (11).

#160727 - $15.00 USD Received 3 Jan 2012; revised 2 Feb 2012; accepted 13 Feb 2012; published 17 Feb 2012

4. Estimation of bit-error rate performance

In Sec.3, we find that the complex amplitude of the beat signal sampled at 1.25 GS/s can completely describe the phase-noise characteristics of DFB and DBR lasers. From such results, we should note the following points: The fast phase fluctuation stemming from the white FM noise is much slower than the sampling rate of 1.25 GS/s, because the intrinsic Lorentzian linewidth is much smaller than the sampling rate. On the other hand, the slow frequency fluctuation due to the low-frequency FM noise remains only in the spectral range below 10 MHz and can well be resolved by 1.25-GS/s sampling, although it induces excess spectral broadening. Therefore, the phase fluctuation of the complex amplitude of the beat can accurately be estimated by 1.25-Gs/s sampling and interpolated within the sampling time interval.

Then we can prepare data samples of the complex amplitude of the beat including the phase noise, which are numerically modulated in an arbitrary format and at an arbitrary symbol rate higher than 1.25 Gsymbol/s. The BER characteristics are finally calculated from such data after Gaussian noise loading. We can thus analyze the phase noise effect on the BER characteristics, using only the beat signal sampled at 1.25 GS/s. The interpolation process is accurate enough for the BER estimation, provided that the sampling rate is ten times higher than the intrinsic Lorentzian spectral width. Once this condition is satisfied, we can cope with any symbol rate, interpolating the sampled complex amplitude.

In this section, we evaluate the BER performance of QPSK and 16-QAM signals at the symbol rate of 10 Gsymbol/s from the complex amplitude of the beat signal sampled at 1.25 GS/s. We consider the following two cases: (1) The two DFB lasers characterized in Sec.3 are used as the transmitter and LO. (2) The DBR laser and one of the DFB lasers are used as the transmitter and LO, respectively.

The procedure of BER calculations is as follows: First, the offset frequency of the complex-amplitude data of the beat signal sampled at 1.25 GS/s is set to zero. Next, the complex-amplitude data with 1.25×10^5 samples are interpolated to form a 10-GS/s data stream with 10^6 samples. The 10-GS/s data are differentially encoded in the QPSK and 16-QAM modulation formats at the symbol rate of 10 Gsymbol/s. Gaussian noise is then loaded to change the energy per bit to noise spectral density ratio E_b/N_0. Carrier-phase estimation is done by the 4-th power algorithm for QPSK [14] and the modified 4-th power algorithm for 16-QAM [15], where the averaging span is optimized to obtain the best BER performance. When the averaging span is too short, the signal-to-noise ratio of the phase reference becomes worse, which results in the BER degradation. On the other hand, when the averaging span is too long, the phase reference cannot follow the actual phase fluctuation and the BER performance is degraded. Thus, the optimum averaging span is dependent on the linewidth of the lasers, the symbol rate of the system, and the modulation format. Finally, symbols are differentially decoded and the number of bit errors is counted. For comparison, we calculate the BER from the data directly obtained by 10-GS/s sampling without interpolation.

Figure 9 shows the BER of the QPSK signal as a function of E_b/N_0 for the case (1) using two DFB lasers. Figure 9(a) represents the BER calculated from the 1.25-GS/s data through the interpolation process, whereas Fig. 9 (b) shows the BER calculated directly from the 10-GS/s data. Red curves are theoretical BERs which do not include the phase-noise effect. Black, green, and blue curves are obtained when the averaging span for carrier-phase estimation is 11, 101, and 1001 symbols, respectively. Since any difference in the BER performance is not observed between Figs. 9 (a) and (b), we find that the 1.25 GS/s data can predict the BER performance at 10 Gsymbol/s. The optimum averaging span is 101 symbols, but the BER is not so sensitive to the averaging span. In addition, the BER degradation by the phase noise is negligibly small. These facts are owing to the sufficiently small phase noise of DFB lasers having the 3-dB linewidth below 100 kHz [3].

#160727 - $15.00 USD Received 3 Jan 2012; revised 2 Feb 2012; accepted 13 Feb 2012; published 17 Feb 2012

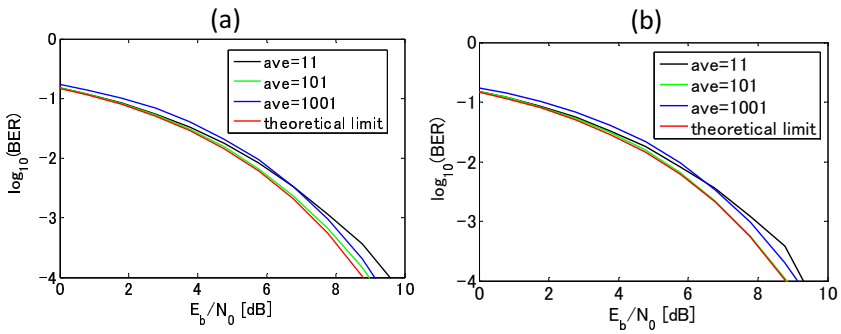

Fig. 9. BER characteristics of the QPSK signal calculated as a function of E_b/N_0 for the case (1) using two DFB lasers. (a):BER calculated from the 1.25-GS/s data through the interpolation process, and (b):BER calculated directly from the 10-GS/s data. Red curves are theoretical BERs which do not include the phase-noise effect. Black, green, and blue curves are obtained when the averaging span for carrier-phase estimation is 11, 101, and 1001 symbols, respectively.

Figure 10 shows the BER of the QPSK signal as a function of E_b/N_0 for the case (2) using DBR and DFB lasers. Figure 10(a) represents the BER calculated from the 1.25-GS/s data through the interpolation process. On the other hand, Fig. 10(b) shows the BER calculated directly from the 10-GS/s data. Red curves are theoretical BERs without the phase-noise effect. Black, green, and blue curves are obtained when the averaging span for carrier-phase estimation is 5, 61, and 201 symbols, respectively. Also in this case, the difference between Figs. 10(a) and 9(b) is not so significant, and we find that the 1.25-GS/s data can be used for calculating the BER performance at 10 Gsymbol/s. When the averaging span is 61 symbols, the BER curve is very close to the theoretical limit. The BER performance in such case is determined from the 600-kHz intrinsic linewidth of the Lorentzian spectrum, and the 600-kHz linewidth is small enough for the 10-GSymbol/s QPSK system [3]. Note that the BER performance is scarcely influenced by the apparent large linewidth. On the other hand, when the averaging span increases beyond this value, the BER degradation becomes remarkable as shown by the blue curves, because the low-frequency FM noise begins to contribute to the carrier-phase estimation process.

Figure 11 shows the BER of the 16-QAM signal as a function of E_b/N_0 for the case (1) using two DFB lasers. Figure 11(a) represents the BER calculated from the 1.25-GS/s data through the interpolation process, whereas Fig. 11 (b) shows the BER calculated directly from the 10-GS/s data. Red curves are BERs when the phase-noise effect is not included. Black, green, and blue curves are obtained when the averaging span for carrier-phase estimation is 11, 51, and 101 symbols, respectively. The difference in the BER performance is not so remarkable between Figs. 11(a) and (b). The optimum averaging span is 51 symbols, and the power penalty at BER=10^{-4} is about 1 dB from the theoretical limit, which is due to the 170-kHz linewidth of the beat.

Figure 12 shows the BER of the 16-QAM signal as a function of E_b/N_0 for the case (2) using DBR and DFB lasers. Figure 12(a) represents the BER calculated from the 1.25-GS/s data through the interpolation process. On the other hand, Fig. 10(b) shows the BER calculated directly from the 10-GS/s data. Red curves represent BERs without the phase-noise effect. Black, green, and blue curves are obtained when the averaging span for carrier-phase estimation is 11, 41, and 101 symbols, respectively. The difference between Figs. 12(a) and 10(b) is not so significant also in this case. When the averaging span is 41 symbols, the power penalty at

#160727 - $15.00 USD Received 3 Jan 2012; revised 2 Feb 2012; accepted 13 Feb 2012; published 17 Feb 2012

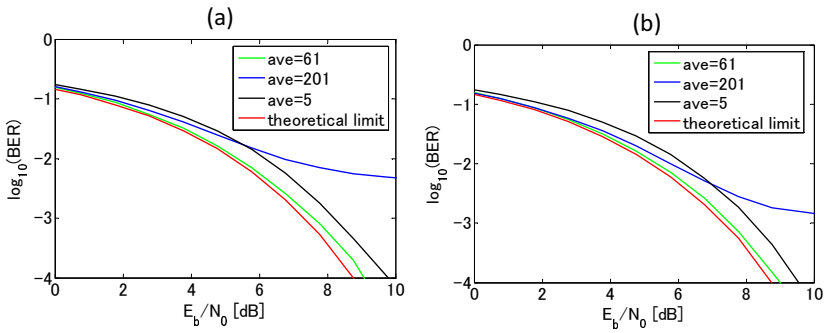

Fig. 10. BER characteristics of the QPSK signal calculated as a function of E_b/N_0 for the case (2) using DBR and DFB lasers. (a):BER calculated from the 1.25-GS/s data through the interpolation process, and (b):BER calculated directly from the 10-GS/s data. Red curves are theoretical BERs which do not include the phase-noise effect. Black, green, and blue curves are obtained when the averaging span for carrier-phase estimation is 5, 61, and 201 symbols, respectively.

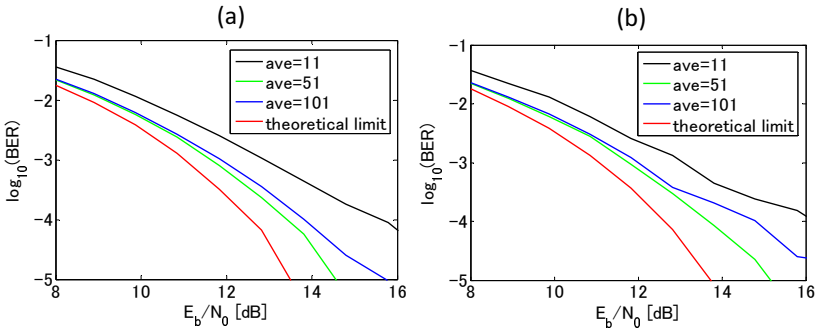

Fig. 11. BER characteristics of the 16-QAM signal calculated as a function of E_b/N_0 for the case (1) using two DFB lasers. (a):BER calculated from the 1.25-GS/s data through the interpolation process, and (b):BER calculated directly from the 10-GS/s data. Red curves are theoretical BERs which do not include the phase-noise effect. Black, green, and blue curves are obtained when the averaging span for carrier-phase estimation is 11, 51, and 101 symbols, respectively.

BER=10^{-4} is about 2 dB, which stems from the 600-kHz intrinsic linewidth of the Lorentzian spectrum. On the other hand, when the averaging span is 101, the BER degradation becomes remarkable as shown by the blue curves, because the effect of the low-frequency FM noise becomes serious.

5. Conclusions

We have presented a systematic method for characterizing the phase noise of semiconductor lasers, using an offline digital coherent receiver. The data on the complex amplitude of the beat signal are sampled and digitized at 1.25 GS/s and sent to the offline digital signal processor. Through digital signal processing, we evaluate the field spectrum, the FM-noise spectrum, and the phase-error variance for different measurement time intervals, which give us full information about the phase-noise characteristics. Lasers under test are DFB and DBR semiconductor lasers. They have significantly different phase-noise characteristics from each other, which orig-

#160727 - $15.00 USD Received 3 Jan 2012; revised 2 Feb 2012; accepted 13 Feb 2012; published 17 Feb 2012

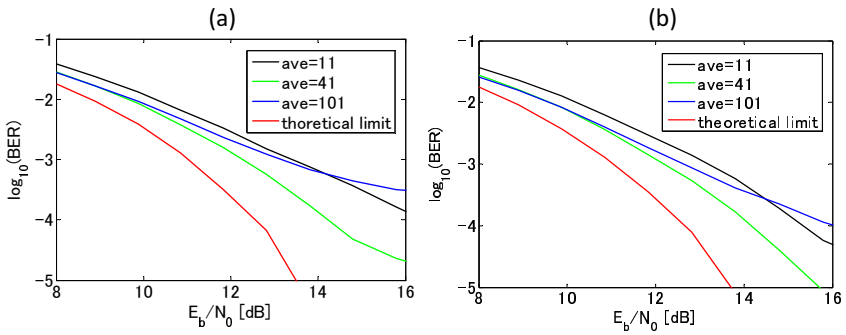

Fig. 12. BER characteristics of the 16-QAM signal calculated as a function of E_b/N_0 for the case (2) using DBR and DFB lasers. (a):BER calculated from the 1.25-GS/s data through the interpolation process, and (b):BER calculated directly from the 10-GS/s data. Red curves are theoretical BERs which do not include the phase-noise effect. Black, green, and blue curves are obtained when the averaging span for carrier-phase estimation is 11, 41, and 101 symbols, respectively.

inate from the difference in the low-frequency FM-noise spectrum. In addition, we show that the BER characteristics at arbitrary-high symbol rates can be estimated from the complex amplitude of the beat sampled at 1.25 GS/s. We calculate BER characteristics of 10-Gsymbol/s QPSK and 16-QAM signals, changing the averaging span for carrier-phase estimation. The dependence of the BER performance on the averaging span is well explained by the measured phase-noise characteristics.

Acknowledgments

The author thanks K. Igarashi of The University of Tokyo for his technical assistance. This work was supported in part by Strategic Information and Communications R&D Promotion Programme (SCOPE) of Ministry of Internal Affairs and Communications, Japan, and Grant-in-Aid for Scientific Research (A) (22246046), the Ministry of Education, Science, Sports and Culture, Japan.

#160727 - $15.00 USD Received 3 Jan 2012; revised 2 Feb 2012; accepted 13 Feb 2012; published 17 Feb 2012